RSC Advances

ROYAL SOCIETY OF CHEMISTRY

www.rsc.org/advances

Journal Name

RSCPublishing

ARTICLE

Biindole-based double D-π-A branched organic dyes for efficient dye-sensitized solar cells

Cite this: DOI: 10.1039/x0xx00000x

Xing Qian, Huan-Huan Gao, Yi-Zhou Zhu,* Lin Lu and Jian-Yu Zheng*

Received 00th January 2012,
Accepted 00th January 2012

DOI: 10.1039/x0xx00000x

www.rsc.org/

A novel class of double D-π-A branched organic dyes based on 2,2′-disubstituted-1*H*,1′*H*-3,3′-biindole moiety have been synthesized, characterized and applied as photosensitizers for dye-sensitized solar cells. Their photophysical, electrochemical and photovoltaic properties are further investigated. These type of organic dyes contain two cyanoacrylic acid moieties as electron acceptors/anchoring groups and different electron-rich conjugated linkers such as furan (**JY11**), thiophene (**JY12**) and 2,2′-bithiophene (**JY13**) as π-bridges. The superiority of the cross X-shaped structure of these double D-π-A branched organic dyes is the suppression of the intermolecular interactions and the guarantee of fast electron injection into the TiO_2 semiconductor in the dye-sensitized solar cells. A highest power conversion efficiency of 6.54% was achieved for **JY13**-based cell with an iodine electrolyte under simulated AM 1.5G solar irradiation (100 mW cm^{-2}).

Introduction

Since the breakthrough work by Grätzel and co-workers, dye-sensitized solar cells (DSSCs) have attracted extensive attention during the past two decades due to their significant potential as low-cost and environmental friendly devices for efficient sunlight-to-electricity conversion.[1] As one of the most important components of DSSCs, sensitizers have shown great influence on light-harvesting, charge transfer and power conversion efficiency (PCE).[2] Recently, several zinc-porphyrin sensitizers, together with Co^{II}/Co^{III} electrolyte, have been designed and successfully applied in DSSC devices to give over 12% PCEs under standard conditions.[3] However, the practical application of porphyrin sensitizer would be inevitably confined by its complex synthetic process and low yield. Alternative metal-free organic dye sensitizers have thus attracted considerable attention for the facile structure tuning, easy synthesis process and low cost.[4]

Donor-π-bridge-acceptor (D-π-A) structure has been commonly involved in most metal-free organic dyes for DSSCs.[5] With an aim of the expansion of the absorption spectra, many single D-π-A dyes have been designed with a long and rod-like configuration, which may facilitate undesirable dye aggregation and charge recombination.[6] The intermolecular π-π stacking of dye molecules often cause self-quenching of excited states and hence inefficient electron injection. Because photovoltage is related to the conduction band level of TiO_2 and the charge recombination rate in DSSCs, such interfacial charge carrier recombination may lead to reduction of photovoltage. Therefore, the suppression of dye aggregation is very important for minimizing the charge recombination and improving photovoltage.[7] To control the intermolecular π-π stacking of organic dyes and related charge recombination processes, several kinds of coadsorbents, such as chenodeoxycholic acid (CDCA), have been physically co-adsorbed on the TiO_2 surface to prevent the intermolecular aggregation of dyes. Another effective strategy is the introducing of long alkyl chains into the dye skeleton, which would diminish the charge recombination between dyes and I_3^- ions in the electrolyte.[8] Employing starburst dyes with bulky multidonor, as well as double D-π-A branched dyes with "X" or "H" shape, has also proved to be effective methods to prevent intermolecular aggregation, retard charge recombination rate and therefore enhance the photovoltage.[9] It was also found that the dye with two D-π-A segments had significantly larger amount of D-π-A segment adsorbed on TiO_2 compared to the single D-π-A dye, which can more effectively suppress the dark current in addition to better light-harvesting and higher photocurrent.[10]

Indole derivatives are important well-known heteroaromatic compounds in diverse natural products and also considered as potential building blocks for functional electroactive materials. Recently, we have incorporated unique discotic triindole to build organic dyes with D-π-A configuration for the first time and an efficiency of 6.1% has been achieved with CDCA as coadsorbent.[11] Because of the highly π-conjugated planar structure, the triindole-based dyes tend to aggregate when anchored on TiO_2 films, which is unfavorable for retarding charge recombination and improving power conversion efficiency. In this report, we present a new extension of double D-π-A branched dyes based on indole derivatives, with the aim of further expanding the possibility of improving the optical and energetic properties of the sensitizers. To the best of our knowledge, the construction of organic dyes with electron-rich 3,3'-biindole core for DSSCs has not been reported yet. So we elaborate the double D-π-A branched dyes that consist of a 1,1'-dioctyl-2,2'-bis(4-(octyloxy)phenyl)-3,3'-biindole moiety acting as the electron donor and two cyanoacylic acid acting as the electron acceptors/anchoring groups. Aromatic π-bridge such as furan, thiophene and 2,2′-bithiophene have been selected to act as the π-conjugated linkers and resulted in sensitizers **JY11**, **JY12** and **JY13**, respectively. The molecular structures of these dyes are shown in Fig. 1.

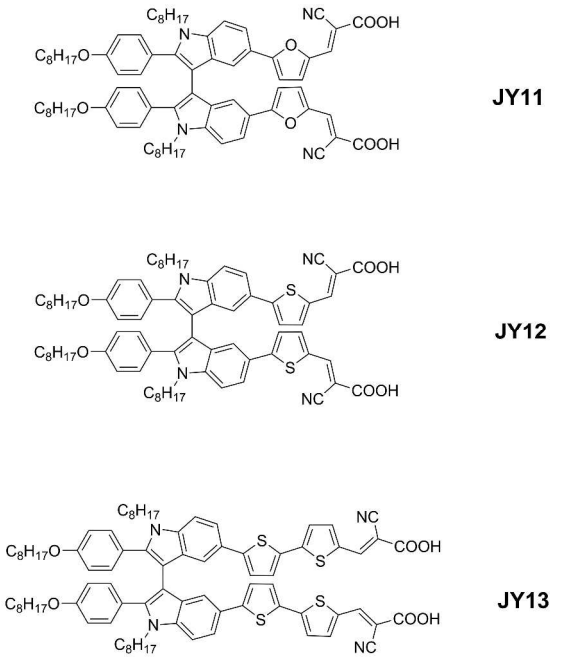

Fig. 1 Chemical structures of the dyes **JY11–13**.

Results and discussion

Molecular design and synthesis

The syntheses of the sensitizers **JY11–13** were achieved in four major steps through a synthetic route displayed in Scheme 1. 2-[(2-Aminophenyl)ethynyl]phenylamine (compound **1**) was prepared according to literature procedure.[12] An acid-catalyzed cascade reaction of compound **1** with 4-octyloxybenzaldehyde afforded 2,2′-disubstituted-1*H*,1′*H*-3,3′-biindole (compound **2**). Alkylation reaction of compound **2** with 1-bromooctane yielded compound **3**. After a bromination of intermediate **3** with NBS and a successive Suzuki cross-coupling with substituted aromatic aldehydes, the π-extended biindole bearing aldehydes **4a–c** were prepared. Finally, the aldehydes **4a–c** were treated with cyanoacetic acid by Knoevenagel reactions to give the dyes **JY11–13**.

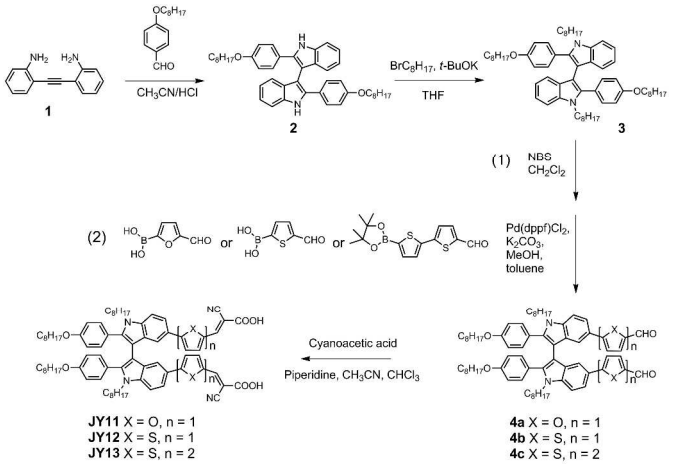

Scheme 1. Synthetic route to **JY11**, **JY12**, and **JY13**.

Photophysical and electrochemical properties

The photophysical characteristics of **JY11**, **JY12** and **JY13** were investigated by UV-vis absorption spectra. The absorption spectra of the three dyes in THF solutions and on TiO_2 films are shown in Fig. 2. As can be seen from Fig. 2a, all dyes exhibit two distinct absorption bands in THF solutions. The absorption bands in the high-energy region (< 370 nm) correspond to the localized aromatic π–π* electron transitions of the conjugated backbone, and the other relatively stronger absorption bands in the low-energy region (> 370 nm) can be assigned to the intramolecular charge transfer (ICT) transitions from the electron donating part to the electron-withdrawing group.[13] The maximum absorption peaks (λ_{max}) for **JY11**, **JY12** and **JY13** are located at 468, 459 and 484 nm, respectively. Furthermore, it can be found that the presence of additional thiophene units in **JY13** (ε = 85170 M^{-1} cm^{-1}) significantly red-shifts its ICT absorption band and results in great enhancement in the molar extinction coefficient relative to **JY11** (ε = 51155 M^{-1} cm^{-1}) and **JY12** (ε = 48914 M^{-1} cm^{-1}), illustrating the importance of extension of electron-rich groups on facilitating the donor-acceptor interactions in dipolar compounds and decreasing the HOMO–LUMO gap of the dyes. As shown in Fig. 2b, when adsorbed on TiO_2, all these dyes showed slight blue-shift absorption peaks as compared to the corresponding spectra recorded in THF solutions. The blue-shift observed for these dyes is due to partial deprotonation of the carboxylic acid unit because of the interaction between the dye and titanium dioxide. The data of absorption and electrochemical properties of these dyes are summarized in Table 1.

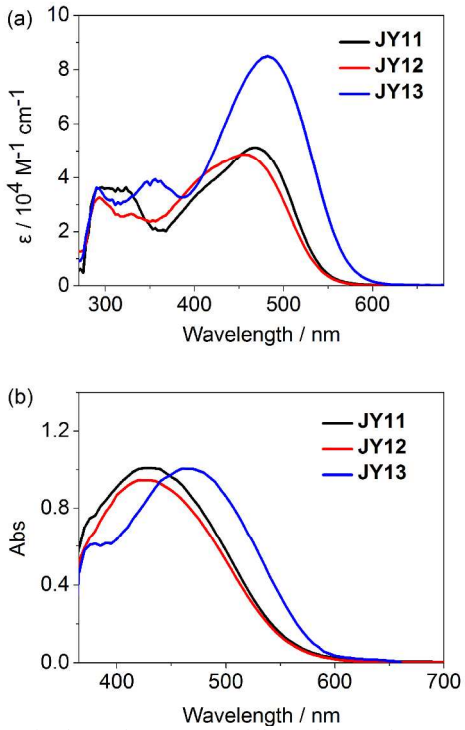

Fig. 2 UV-vis absorption spectra of these dyes (a) in THF solutions and (b) on TiO_2 films.

To evaluate the possibility of electron injection from the excited state dye to the conduction band (CB) of TiO_2 and dye regeneration on TiO_2 electrode, cyclic voltammetry measurement was performed in benzonitrile solution with a 100 mV s^{-1} scan rate and calibrated against ferrocene, using 0.1 M

tetrabutylammonium hexafluorophosphate as the supporting electrolyte. Cyclic voltammograms of the dyes are depicted in Fig. 3. As shown in Fig. 3, all three dyes exhibited two reversible oxidation couples. The highest occupied molecular orbitals (HOMOs) of **JY11**–**13** corresponding to their first oxidation potentials (E_{ox}) were 0.88, 0.89 and 0.83 V (*vs.* NHE), respectively. The band gap energies (E_{0-0}) of the three dyes **JY11**–**13** were 2.07, 2.09 and 1.98 eV, respectively, which were calculated from their onset wavelength in absorption spectra in THF solutions. The lowest unoccupied molecular orbitals (LUMOs) of **JY11**–**13**, which could be calculated from $E_{ox} - E_{0-0}$, were –1.19, –1.20 and –1.15 V (*vs.* NHE), respectively. Consequently, the LUMO levels of **JY11**–**13** are all more negative than the CB of the TiO_2 electrode (−0.5 V *vs.* NHE), indicating that electron injection from the LUMO orbital into the CB of TiO_2 is energetically permitted. On the other hand, the HOMO levels of **JY11**–**13** are sufficiently more positive than the I^-/I_3^- redox couple (+0.4 V *vs.* NHE), ensuring the thermodynamic regeneration of the oxidized form of the dyes in a DSSC.

Table 1 Photophysical, electrochemical data of **JY11**–**13**.[a]

Dye	λ_{max} /nm	ε/M^{-1} cm^{-1}	E_{ox}/V	E_{0-0}/eV	E_{red}/ V	HOMO/ LUMO/eV
JY11	468	51155	0.88	2.07	−1.19	−5.38/−3.31
JY12	459	48914	0.89	2.09	−1.20	−5.39/−3.30
JY13	484	85170	0.83	1.98	−1.15	−5.33/−3.35

[a] First oxidation potentials (*vs.* NHE) in benzonitrile were calibrated with ferrocene (0.63 V *vs.* NHE).[14] E_{0-0} values (zeroth-zeroth transition energies) were estimated from the onset wavelength in absorption spectra in THF. $E_{red} = E_{ox} - E_{0-0}$. NHE *vs.* the vacuum level was set to 4.5 V.[15]

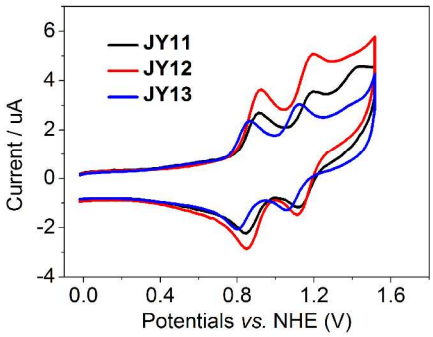

Fig. 3 Cyclic voltammograms of the dyes recorded in benzonitrile solutions.

Computational analysis

To deep investigate the geometrical structures and the frontier molecular orbital configurations of the three double D-π-A type dyes, density functional theory calculations were conducted with the Gaussian 03 program at the B3LYP/6-31G(d) level. All octyl groups have been replaced with methyl groups to save calculation time. The optimized geometries and frontier molecular orbital distributions of three dyes are shown in Fig. 4. Optimized geometry demonstrated all dyes present a "X" shape, which benefits the suppression of electron recombination and improvement of open-circuit voltage. Notably, the intersection angle of the two D-π-A branches of **JY11** (88°) is more closer to vertical angle as compared to that of **JY12** (79°) and **JY13** (64°), which indicates a weaker intermolecular aggregation of **JY11** and the cell based on **JY11** may have a relative higher open-circuit voltage. As shown in Fig. 4, for the HOMOs of all dyes, the electron density is uniformly distributed on biindole core. For the HOMO–1 state, the electron density is almost distributed on single D-π-A branch. At the meantime, the LUMO and LUMO–1 of these dyes are very similar, and the electron density shows localized electron distributions through the each single cyanoacrylic acid unit and its adjacent π-spacer. Because the HOMO, HOMO–1, LUMO and LUMO+1 are more important than other orbitals because their electron transitions are very favorable for the photon-to-electron conversion and the electron may be easily transferred from the HOMO and HOMO–1 to the LUMO and LUMO+1 and then be injected into the semiconductor. Therefore, these electron distributions will preferentially ensure that electrons will be efficient transferred from the biindole core through the electron-rich π-space to the cyanoacrylic acid acceptor. From the analysis of the TD-DFT results in Table 2, we can assign the ICT absorption peaks of the three dyes as transitions from HOMO–1, HOMO–2 and HOMO–3 to LUMO and LUMO+1. The electronic transitions in the three dyes are positively contributed to electron injection since ICT transitions correspond to electron transfer from the whole molecule to the anchoring group. The order of calculated absorption peaks and absorption intensity of these dyes are also similarly ranked as those of experimental values.

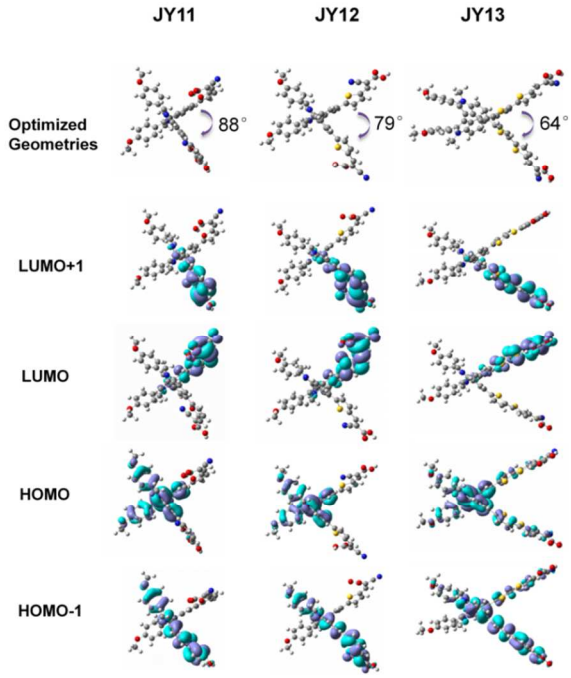

Fig. 4 The optimized geometries and frontier molecular orbital distributions of three dyes optimized by DFT calculations.

Table 2 Excitation wavelengths, orbital energies, oscillator strength (*f*) and assignment of the dyes in vacuum computed using B3LYP.

Dye	λ_{max} /nm	Calculated energy/eV	*f*	Transition assignment[a]
JY11	431	2.88	0.62	H–3 → L (70%) H–2 → L (9%)
JY12	428	2.90	0.60	H–1 → L+1 (33%) H–3 → L (18%) H–2 → L+1 (17%) H–2 → L (15%)
JY13	489	2.54	1.41	H–1 → L+1 (41%) H–2 → L (28%)

[a] H = HOMO, L = LUMO.

DSSC performance

The photovoltaic characteristics of the DSSCs based on the three dyes under simulated AM 1.5G solar irradiation (100 mW cm^{-2}) have been investigated, employing a liquid electrolyte composed of 0.3 M 1,2-dimethyl-3-propylimidazolium iodide (DMPII), 0.1 M LiI, 0.05 M I_2, and 0.5 M 4-*tert*-butyl pyridine (TBP) in acetonitrile. The DSSCs performance parameters of **JY11**−**13** and commercial **N719** dye are displayed in Table 3. The photocurrent density-voltage (*J-V*) curves of **JY11**−**13** are plotted in Fig. 5a. The **JY12** dye exhibited a short-circuit photocurrent density (J_{sc}) of 14.0 mA cm^{-2}, an open-circuit photovoltage (V_{oc}) of 674 mV and a fill factor (FF) of 0.64, generating a PCE of 6.05%. The **JY11** dye showed a 27 mV improved V_{oc} benefitting from its nearly vertical intersection angle of the two D-π-A branches as compared to that of **JY12**, which endowed **JY11** the potential of reduced intermolecular π-π stacking. Nevertheless, the **JY11** dye displayed a lower J_{sc} of 12.7 mA cm^{-2} and a FF of 0.66, resulting in a slightly reduced PCE of 5.87%. Notably, **JY13** exhibited a lowest V_{oc} (663 mV) and a lowest FF of 0.62 with the extension of π-bridge compared to **JY11** and **JY12**. But greatly benefited from its broader and more intense ICT band, **JY13** finally displayed a relatively higher J_{sc} of 15.8 mA cm^{-2} and an increased PCE of 6.54%.

Table 3 Photovoltaic performance of **JY11**–**13** with **N719** as a reference.[a]

Dye	V_{oc}/mV	J_{sc}/mA cm^{-2}	FF	PCE/%
JY11	701	12.7	0.66	5.87
JY12	674	14.0	0.64	6.05
JY13	663	15.8	0.62	6.54
N719	765	17.2	0.62	8.20

[a] Active area was 0.196 cm^2 with a metal mask; Used an electrolyte composed of 0.3 M 1,2-dimethyl-3-propylimidazolium iodide (DMPII), 0.1 M LiI, 0.05 M I_2, and 0.5 M 4-*tert*-butyl pyridine in acetonitrile; Applied the commercial **N719** dye for comparison.

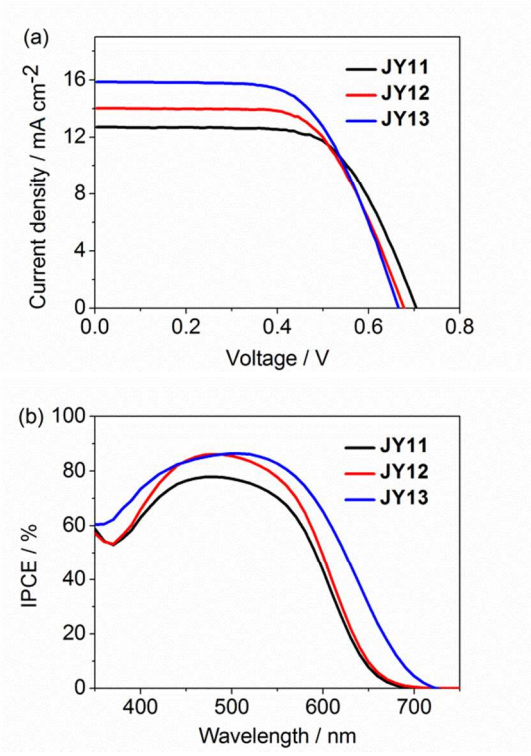

Fig. 5 (a) The photocurrent density-voltage (*J-V*) curves and (b) the IPCE spectra of **JY11–13**.

In order to analyze the difference between the J_{sc} values of the three dyes, the incident photon-to-current conversion efficiencies (IPCE) as a function of incident wavelength for DSSCs based on these dyes are plotted in Figure 5b. As shown in IPCE spectra, all of the dyes **JY11**−**13** could efficiently convert the light to photocurrents in the UV-vis region and the onsets of the IPCE spectra for the three dyes were at 690, 700 and 720 nm, respectively. **JY13**-based cell gave over 60% IPCE values from 350 to 610 nm with a maximum IPCE value of 86% at 500 nm, which ensured a good light-harvesting ability and a high photocurrent. The high IPCE value and broader absorption of **JY13** explained the high J_{sc} value from the *J-V* measurement. The somewhat higher efficiency observed for **JY13** was mainly due to the relatively larger J_{sc}. The best efficiency of **JY13**-based cell reached about 80% of the commercial **N719**-based standard cell that fabricated and measured under the same conditions, indicating the 3,3′-biindole skeleton is a promising candidate to construct effective double D-π-A branched organic dyes for DSSCs.

Electrochemical impedance spectroscopy

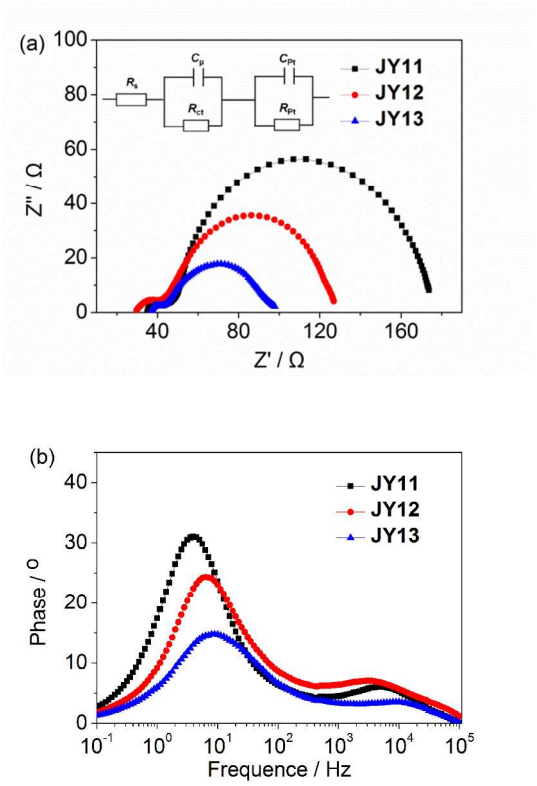

Fig. 6 (a) Nyquist plots and (b) Bode phase plots for DSSCs based on the three dyes measured in the dark under -0.65 V bias.

Electrochemical impedance spectroscopy (EIS) is a powerful technique of characterizing the important interfacial charge transfer and carrier transportation process in DSSCs.[16] EIS Nyquist plots and Bode phase plots of DSSCs based on **JY11**, **JY12** and **JY13** measured in the dark under forward bias (–0.65 V) with frequency range of 100 kHz to 100 mHz are shown in Fig. 6. In the Nyquist plots, the larger semicircle in the lower frequency range represents the interfacial charge transfer

resistances (R_{ct}) at the TiO_2/dyes/electrolyte interface.[17] A larger radius of the major semicircle means a larger charge transfer resistance, indicating that the electron recombination in the devices are strongly reduced and therefore a smaller dark current and a larger value of photovoltage.[18] The fitted R_{ct} increased in the order of **JY13** (44 Ω) < **JY12** (77 Ω) < **JY11** (120 Ω). This trend appeared to be consistent with the values of V_{oc} of **JY13** (663 mV) < **JY12** (674 mV) < **JY11** (701 mV). Besides, electron lifetime (τ) can be extracted from the chemical capacitance (C_μ) and R_{ct} using $\tau = R_{ct} \times C_\mu$.[19] In general, longer electron lifetime implies increased resistance between the injected electrons and the electrolyte, which consequently improves the V_{oc}.[20] The electron lifetime was in the order with the calculated values of **JY13** (24.5 ms) < **JY12** (34.4 ms) < **JY11** (70.1 ms). So the higher V_{oc} of **JY11** could be further explained.

Conclusions

In conclusion, three novel double D-π-A branched organic dyes **JY11**, **JY12** and **JY13** composed of biindole donors, cyanoacrylic acid acceptors and aromatic π-bridges have been successfully designed, synthesized and applied as photosensitizers for DSSCs. Most importantly, the double D-π-A branched biindole dyes exhibit X-shaped structure, which is favorable for the suppression of the intermolecular interactions and finally results in the reduced charge recombination rates as well as good light-harvesting, large photocurrent and high PCE values in DSSCs. All three sensitizers have shown significant performance in DSSCs. The key difference of the photophysical characteristics among the three sensitizers locates at the absorption properties where a broader and more intense ICT band can be observed for sensitizer **JY13** with bithiophene as the π-linker. The PCE value of the solar cell based on **JY13** is up to 6.54%. This work emphasizes the potential of the application of double D-π-A branched biindole dyes for efficient DSSCs. Work focusing on the molecular modification of X-shape dye is ongoing in our lab.

Experimental

Materials and methods

All solvents were purified according to standard methods. Other chemicals (AR) obtained from commercial sources were used without any further purification. NMR solvents were used as received. ^{1}H NMR and ^{13}C NMR spectra were recorded on Bruker 400 MHz spectrometer using TMS as the internal standard. UV-vis spectra were obtained on a Varian Cary 300 Conc UV-visible spectrophotometer. HR-MS data was obtained on a Varian 7.0T FTMS. Cyclic voltammetry experiments and electrochemical impedance spectroscopy (EIS) were recorded on an electrochemical workstation (Zennium, Zahner Corporation). Cyclic voltammetry experiments were carried out using a conventional three-electrode system employing a glassy carbon electrode as the working electrode, a Ag/Ag^+ electrode as the reference electrode, and a Pt wire as the counter electrode. The redox potentials were measured in dichloromethane, using 0.1 M n-Bu_4NPF_6 as the supporting electrolyte with a scan rate of 100 mV S^{-1}.

Fabrication and characterization of DSSCs

A TiO_2 film (~10 μm) for the transparent nanocrystalline layer was prepared according to the doctor-blade method by coating a commercial 20 nm TiO_2 sol (China National Academy of Nanotechnology & Engineering) onto the treated FTO conductive glass (Nippon Sheet Glass, Japan, fluorine-doped SnO_2 over layer, sheet resistance of 15 Ω/sq, treated with $TiCl_4$ (0.05 M) aqueous solution). The scattering layer (~4 μm) was applied over the transparent layer by doctor-blade method, then gradually heated to 500°C and sintered for 60min. The resulting TiO_2 electrodes were treated by $TiCl_4$ (0.04 M) aqueous solution at 70°C for 60 min and sintered again at 500°C for 60min. The Pt electrode was obtained by thermal deposition a platinum layer on the surface of FTO at 450°C for 30 min. The TiO_2 photoanodes were immersed in the commercial **N719** dye solution (0.3 mM in ethanol) for 12 h. The adsorption of the biindole-based dyes on TiO_2 was carried out with 0.3 mM dye solution in THF for 12 h. The electrolyte was composed of 0.3 M DMPII, 0.1 M LiI, 0.05 M I_2, and 0.5 M 4-*tert*-butylpyridine in acetonitrile. The DSSCs were illuminated by a solar simulator (CHF-XM-500W, Trusttech Co. Ltd.) under 100 mW/cm^2 irradiation, which was calibrated by a standard silicon solar cell (91150V, Newport Corporation). The photocurrent intensity-voltage (*J-V*) characteristic curves of the DSSC under simulated sunlight were recorded using an electrochemical workstation (Zennium, Zahner Corporation). The measurement of the incident photon-to-current conversion efficiency (IPCE) was performed using a commercial setup (QTest Station 2000 IPCE Measurement System, CROWNTECH, USA).

Synthetic procedures

Synthesis of compound 2. Compound **2** was prepared according to literature procedure.[12] To the solution of 2-[(2-aminophenyl)ethynyl]phenylamine (compound **1**) (0.50 g, 2.4 mmol) and 4-octyloxybenzaldehyde (1.69 g, 7.2 mmol) in CH_3CN (35 mL) was added concentrated hydrochloric acid (0.1 mL, 37% aqueous solution). The mixture was stirred at reflux and monitored by TLC. After 1h, the solvent was evaporated and the residue was purified by silica-gel column chromatography(eluent: hexane/EtOAc = 95:5) to afford compound **2** as a pale yellow solid (yield: 82.0%). ^{1}H NMR (400 MHz, acetone-*d*6) δ 10.58 (s, 2H), 7.51 (d, *J* = 8.6 Hz, 4H), 7.46 (d, *J* = 8.4 Hz, 2H), 7.13–7.03 (m, 4H), 6.87 (t, *J* = 7.5 Hz, 2H), 6.71 (d, *J* = 8.7 Hz, 4H), 3.87 (t, *J* = 6.5 Hz, 4H), 1.73–1.62 (m, 4H), 1.43–1.25 (m, 20H), 0.86 (t, *J* = 6.5 Hz, 6H). ^{13}C NMR (101 MHz, acetone-*d*6) δ 158.34, 136.71, 135.17, 130.32, 127.86, 125.81, 121.54, 119.54, 119.11, 114.25, 110.92, 105.88, 67.50, 31.69, 29.14, 29.08 , 28.43, 25.87, 22.44, 13.51.

Synthesis of compound 3. *t*-BuOK (0.97 g,8.6 mmol) was added to a solution of compound **2** (1.54g, 2.4 mmol) in dry THF (30 mL), and the resulting mixture was stirred at room temperature for 0.5 h. 1-Bromooctane (1.86 g, 9.6 mmol) was then added, and the mixture was heated at reflux for another 3 hours before evaporated. The crude product was purified by silica-gel column chromatography using CH_2Cl_2/petroleum ether (1:4) as the eluent to afford compound **3** as a colorless oil liquid (yield: 73.2%). ^{1}H NMR (400 MHz, $CDCl_3$) δ 7.56 (d, *J* = 7.8 Hz, 2H), 7.43 (d, *J* = 8.1 Hz, 2H), 7.25 (s, 2H), 7.12 (t, *J* = 7.4 Hz, 2H), 6.67 (d, *J* = 8.3 Hz, 4H), 6.63 (d, *J* = 8.3 Hz, 4H), 4.03 (t, *J* = 7.1 Hz, 4H), 3.94 (t, *J* = 6.4 Hz, 4H), 1.87–1.75 (m, 4H), 1.56–1.47 (m, 4H), 1.41–1.11 (m, 40H), 0.95–0.85 (m, 12H). ^{13}C NMR (101 MHz, $CDCl_3$) δ 158.05, 138.69, 136.54, 131.36, 129.56, 124.89, 120.96, 120.72, 118.91, 113.82, 109.62, 107.42, 67.96, 43.86, 31.88, 31.77, 29.80, 29.46, 29.33, 29.15, 29.06, 27.62, 26.74, 26.13, 22.72, 22.64, 14.16, 14.13. HR-MS (MALDI): m/z $[M]^+$ calcd for $C_{60}H_{84}N_2O_2$, 864.6533, found, 864.6528.

Synthesis of compound 4a. A solution of *N*-bromosuccinimide (NBS) (166 mg, 0.93 mmol) in CH_2Cl_2 (15 mL) was added dropwise to a solution of compound **3** (402 mg, 0.46 mmol) in CH_2Cl_2 (40 mL) at 0 °C. The mixture was then slowly warmed to room temperature and stirred for 1 h before it was poured into water. The organic phase was separated and dried over anhydrous Na_2SO_4. After the solvent was evaporated, the crude product was transferred to a two-neck round-bottomed flask. Then, 5-formylfuran-2-boronic acid (167 mg, 1.20 mmol), $Pd(dppf)Cl_2$ (38 mg, 0.046 mmol), K_2CO_3 (730 mg, 2.30 mmol), toluene (15 mL) and methanol (5 mL) were added. The flask was charged with N_2. The mixture was reflux for 5 h before it was poured into water. The organic phase was separated and dried over anhydrous Na_2SO_4. After the solvent was removed under vacuum, the crude product was purified by silica-gel column chromatography using CH_2Cl_2 as the eluent to afford compound 4**a** as an orange thickness liquid (yield: 76.4%). ^{1}H NMR (400 MHz, $CDCl_3$) δ 9.64 (s, 2H), 7.95 (s, 2H), 7.54–7.45 (m, 4H), 7.38 (s, 2H), 6.88 (s, 2H), 6.72 (d, *J* = 8.1 Hz, 4H), 6.66 (d, *J* = 7.9 Hz, 4H), 4.13 (t, *J* = 7.0 Hz, 4H), 3.94 (t, *J* = 6.3 Hz, 4H), 1.85–1.76 (m, 4H), 1.54–1.45 (m, 4H), 1.39–1.07 (m, 40H), 0.92 (t, *J* = 5.8 Hz, 6H), 0.86 (t, *J* = 7.0 Hz, 6H). ^{13}C NMR (101 MHz, $CDCl_3$) δ 176.63, 161.97, 158.50, 151.56, 141.46, 136.60, 131.14, 130.66, 124.03, 121.96, 120.69, 117.26, 114.05, 107.61, 107.06, 106.72, 68.00, 43.94, 31.85, 31.73, 29.87, 29.72, 29.43, 29.29, 29.09, 28.98, 26.58, 26.10, 22.69, 22.61, 14.13, 14.10. HR-MS (MALDI): m/z $[M]^+$ calcd for $C_{70}H_{88}N_2O_6$, 1052.6642, found, 1052.6662.

Synthesis of compound 4b. The synthesis method resembles that of compound **4a** and the compound was purified by silica-gel column chromatography using CH_2Cl_2 as the eluent to afford compound **4b** as an orange thickness liquid (yield: 80.2%). ^{1}H NMR (400 MHz, $CDCl_3$) δ 9.88 (s, 2H), 7.73 (d, *J* = 17.9 Hz, 4H), 7.51 (d, *J* = 8.1 Hz, 2H), 7.44 (d, *J* = 8.4 Hz, 4H), 6.69 (d, *J* = 8.4 Hz, 4H), 6.65 (d, *J* = 8.1 Hz, 4H), 4.07 (t, *J* = 7.0 Hz, 4H), 3.93 (t, *J* = 5.9 Hz, 4H), 1.84–1.76 (m, 4H), 1.53–1.45 (m, 4H), 1.39–1.11 (m, 40H), 0.90 (t, *J* = 6.4 Hz, 6H), 0.85 (t, *J* = 6.8 Hz, 6H). ^{13}C NMR (101 MHz, $CDCl_3$) δ 182.66, 158.50, 157.04, 141.25, 141.16, 137.90, 136.70, 131.14, 130.53, 126.26, 123.96, 123.12, 120.88, 118.22, 114.06, 108.08, 107.47, 68.01, 44.00, 31.87, 31.75, 29.85, 29.74, 29.44, 29.31, 29.12, 29.00, 26.68, 26.12, 22.71, 22.64, 14.16, 14.14. HR-MS (MALDI): m/z $[M]^+$ calcd for $C_{70}H_{88}N_2O_4S_2$, 1084.6186, found, 1084.6210.

Synthesis of compound 4c. The synthesis method resembles that of compound **4a** and the compound was purified by silica-gel column chromatography using CH_2Cl_2 as the eluent to afford compound **4c** as a red thickness liquid (yield: 70.5%). ^{1}H NMR (400 MHz, $CDCl_3$) δ 9.85 (s, 2H), 7.67 (d, *J* = 3.8 Hz, 2H), 7.61 (s, 2H), 7.50 (d, *J* = 8.2 Hz, 2H), 7.38 (dd, *J* = 4.9, 2.5 Hz, 4H), 7.31 (d, *J* = 3.8 Hz, 2H), 7.27 (d, *J* = 3.9 Hz, 2H), 6.67 (d, *J* = 8.7 Hz, 4H), 6.63 (d, *J* = 8.8 Hz, 4H), 4.05 (t, *J* = 6.8 Hz, 4H), 3.91 (t, *J* = 6.5 Hz, 4H), 1.85–1.73 (m, 4H), 1.51–1.43 (m, 4H), 1.40–1.10 (m, 40H), 0.89 (t, *J* = 6.7 Hz, 6H), 0.84 (t, *J* = 7.1 Hz, 6H). ^{13}C NMR (101 MHz, $CDCl_3$) δ 182.43, 158.37, 148.70, 147.79, 141.06, 140.53, 137.57, 136.79, 133.75, 131.19, 129.73, 127.31, 126.77, 124.22, 123.57, 123.24, 120.89, 117.93, 114.00, 107.49, 107.26, 68.01, 43.91, 31.86, 31.77, 29.80, 29.73, 29.44, 29.40, 29.31, 29.12, 28.99, 26.67, 26.11, 22.70, 22.65, 14.14. HR-MS (MALDI): m/z $[M]^+$ calcd for $C_{78}H_{92}N_2O_4S_4$, 1248.5940, found, 1248.5938.

Synthesis of JY11. A mixture of compound **4a** (80 mg, 0.15 mmol), cyanoacetic acid (38 mg, 0.45 mmol), piperdine (0.10 mL), $CHCl_3$ (10 mL) and CH_3CN (10 mL) was heated at reflux for 12 h and then acidified with 2 M aqueous hydrochloric acid (10 ml). The crude product was extracted into $CHCl_3$, and the organic layer was washed with water and dried over anhydrous Na_2SO_4. After removal of the solvent under reduced pressure, the crude product was purified by silica-gel column chromatography using CH_2Cl_2/CH_3OH (8:1) as the eluent to afford **JY11** as a red solid (yield: 80.5%). ^{1}H NMR (400 MHz, DMSO-d_6) δ 8.14 (s, 2H), 8.04 (s, 2H), 7.54 (d, *J* = 3.4 Hz, 2H), 7.50 (d, *J* = 8.3 Hz, 2H), 7.31 (d, *J* = 3.3 Hz, 2H), 7.15 (d, *J* = 8.4 Hz, 2H), 6.95 (d, *J* = 8.2 Hz, 4H), 6.73 (d, *J* = 8.2 Hz, 4H), 4.23–4.04 (m, 4H), 3.87 (t, *J* = 5.3 Hz, 4H), 1.72–1.61 (m, 4H), 1.59–1.49 (m, 4H), 1.39–1.32 (m, 4H), 1.29–1.19 (m, 16H), 1.18–1.11 (m, 4H), 1.09–0.95 (m, 16H), 0.83 (t, *J* = 6.4 Hz, 6H), 0.77 (t, *J* = 7.1 Hz, 6H). ^{13}C NMR (101 MHz, DMSO-*d*6) δ 164.69, 161.34, 158.60, 147.31, 141.72, 139.64, 137.70, 136.76, 131.27, 130.01, 125.36, 123.83, 121.99, 120.32, 117.56, 117.26, 114.46, 109.22, 107.54, 96.16, 67.68, 34.84, 31.70, 31.59, 30.86, 29.19, 29.16, 29.01, 28.94, 28.62, 26.12, 25.96, 22.55, 22.50, 14.36, 14.32. HR-MS (MALDI): m/z $[M]^+$ calcd for $C_{76}H_{90}N_4O_8$, 1186.6759, found, 1186.6755.

Synthesis of JY12. JY12 was synthesized according to the procedure described for **JY11** and the compound was purified by silica-gel column chromatography using CH_2Cl_2/CH_3OH (8:1) as the eluent to afford **JY12** as a red solid (yield: 82.1%). ^{1}H NMR (400 MHz, DMSO-d_6) δ 8.47 (s, 2H), 8.08–7.95 (m, 4H), 7.80 (d, *J* = 3.9 Hz, 2H), 7.32 (d, *J* = 8.5 Hz, 2H), 7.17 (d, *J* = 8.3 Hz, 2H), 6.88 (d, *J* = 8.4 Hz, 4H), 6.73 (d, *J* = 8.6 Hz, 4H), 4.25–4.07 (m, 4H), 3.89 (t, *J* = 6.2 Hz, 4H), 1.72–1.62 (m, 4H), 1.55–1.46 (m, 4H), 1.41–1.33 (m, 4H), 1.29–1.21 (m, 16H), 1.17–1.10 (m, 4H), 1.06–0.92 (m, 16H), 0.84 (t, *J* = 6.6 Hz, 6H), 0.77 (t, *J* = 7.2 Hz, 6H). ^{13}C NMR (101 MHz, DMSO-*d*6) δ 164.30, 158.62, 155.94, 146.82, 141.99, 141.75, 136.92, 133.90, 131.27, 130.20, 126.04, 124.59, 123.90, 120.54, 118.62, 117.28, 114.53, 108.79, 107.45, 97.78, 67.75, 43.48, 31.70, 31.57, 29.43, 29.19, 29.15, 29.02, 28.92, 28.63, 26.12, 25.96, 22.55, 22.49, 14.39, 14.35. HR-MS (MALDI): m/z $[M]^+$ calcd for $C_{76}H_{90}N_4O_6S_2$, 1218.6302, found, 1218.6297.

Synthesis of JY13. JY13 was synthesized according to the procedure described for **JY11** and the compound was purified by silica-gel column chromatography using CH_2Cl_2/CH_3OH (6:1) as the eluent to afford **JY13** as a deep red solid (yield: 85.2%). ^{1}H NMR (400 MHz, DMSO-d_6) δ 8.46 (s, 2H), 7.95 (d, *J* = 3.9 Hz, 2H), 7.87 (s, 2H), 7.60 (d, *J* = 3.4 Hz, 2H), 7.56 (d, *J* = 3.5 Hz, 2H), 7.54 (d, *J* = 3.7 Hz, 2H), 7.25 (d, *J* = 8.1 Hz, 2H), 7.12 (d, *J* = 8.1 Hz, 2H), 6.82 (d, *J* = 8.1 Hz, 4H), 6.68 (d, *J* = 8.1 Hz, 4H), 4.39–4.03 (m, 4H), 3.96–3.73 (m, 4H), 1.75–1.55 (m, 4H), 1.58–1.40 (m, 4H), 1.37–0.93 (m, 40H), 0.81 (t, *J* = 6.8 Hz, 6H), 0.75 (t, *J* = 7.1 Hz, 6H). ^{13}C NMR (101 MHz, DMSO-*d*6) δ 164.13, 158.51, 148.24, 146.61, 146.54, 141.98, 140.89, 137.01, 133.97, 133.17, 131.28, 129.47, 128.78, 126.57, 124.83, 124.70, 124.13, 120.36, 118.04, 117.16, 114.45, 107.93, 107.41, 98.30, 67.75, 43.40, 31.71, 31.60, 29.45, 29.21, 29.16, 29.05, 28.93, 28.66, 26.14, 25.98, 22.55, 22.50, 14.37, 14.34. HR-MS (MALDI): m/z $[M]^+$ calcd for $C_{84}H_{94}N_4O_6S_4$, 1382.6056, found, 1382.6050.

Acknowledgements

We are grateful to the 973 Program (2011CB932502), and the National Natural Science Foundation of China (Nos: 21172126 and 21272123) for their generous financial support.

Notes and references

State Key Laboratory and Institute of Elemento-Organic Chemistry, Collaborative Innovation Center of Chemical Science and Engineering (Tianjin), Nankai University, Tianjin 300071, China. E-mail: zhuyizhou@nankai.edu.cn; jyzheng@nankai.edu.cn. Fax: +86-22-2350 5572; Tel: +86-22-2350 5572.

† Electronic Supplementary Information (ESI) available: NMR spectra of all new compounds. See DOI: 10.1039/b000000x/

1 B. O'Regan and M. Grätzel, *Nature*, 1991, **353**, 737–740.

2 (a) M. Grätzel, *Acc. Chem. Res.*, 2009, **42**, 1788–1798; (b) J. Mao, N. He, Z. Ning, Q. Zhang, F. Guo, L. Chen, W. Wu, J. Hua and H. Tian, *Angew. Chem. Int. Ed.*, 2012, **51**, 9873–9876.

3 (a) A. Yella, H.-W. Lee, H. N. Tsao, C. Yi, A. K. Chandiran, M. K. Nazeeruddin, E. W.-G. Diau, C.-Y. Yeh, S. M. Zakeeruddin and M. Grätzel, *Science*, 2011, **334**, 629–633; (b) A. Yella, C.-L. Mai, S. M. Zakeeruddin, S.-N. Chang, C.-H. Hsieh, C.-Y. Yeh and M. Grätzel, *Angew. Chem. Int. Ed.*, 2014, **53**, 2973–2977; (c) S. Mathew, A. Yella, P. Gao, R. Humphry-Baker, B. F. E. Curchod, N. Ashari-Astani, I. Tavernelli, U. Rothlisberger, M. K. Nazeeruddin and M. Grätzel, *Nat. Chem.*, 2014, **6**, 242–247.

4 (a) A. Hagfeldt, G. Boschloo, L. Sun, L. Kloo and H. Pettersson, *Chem. Rev.*, 2010, **110**, 6595–6663; (b) M. Liang and J. Chen, *Chem. Soc. Rev.*, 2013, **42**, 3453–3488; (c) N. Cai, J. Zhang, M. Xu, M. Zhang and P. Wang, *Adv. Funct. Mater.*, 2013, **23**, 3539–3547; (d) K. Ladomenou, T. N. Kitsopoulos, G. D. Sharma and A. G. Coutsolelos, *RSC Adv.*, 2014, **4**, 21379–21404; (d) E. Gabrielsson, H. Ellis, S. Feldt, H. Tian, G. Boschloo, A. Hagfeldt and L. Sun, *Adv. Energy Mater.*, 2013, **3**, 1647–1656.

5 (a) Z. Wang, M. Liang, Y. Hao, Y. Zhang, L. Wang, Z. Sun and S. Xue, *J. Mater. Chem. A*, 2013, **1**, 11809–11819; (b) J. Zhao, X. Yang, M. Cheng, S. Li, X. Wang and L. Sun, *J. Mater. Chem. A*, 2013, **1**, 2441–2446. (c) Y. Tan, M. Liang, Z. Lu, Y. Zheng, X. Tong, Z. Sun and S. Xue, *Org. Lett.*, 2014, **16**, 3978–3981; (d) Z. Yao, L. Yang, Y. Cai, C. Yan, M. Zhang, N. Cai, X. Dong and P. Wang, *J. Phys. Chem. C*, 2014, **118**, 2977–2986. (e) X. Guo, H. N. Tsao, P. Gao, D. Xia, C. An, M. K. Nazeeruddin, M. Baumgarten, M. Grätzel and K. Müllen, *RSC Adv.*, 2014, **4**, 54130–54133.

6 A. Baheti, K. R. J. Thomas, C.-P. Lee, C.-T. Li and K.-C. Ho, *J. Mater. Chem. A*, 2014, **2**, 5766–5779;

7 (a) X. Ren, S. Jiang, M. Cha, G. Zhou and Z.-S. Wang, *Chem. Mater.*, 2012, **24**, 3493–3499; (b) M. Cai, X. Pan, W. Liu, J. Sheng, X. Fang, C. Zhang, Z. Huo, H. Tian, S. Xiao and S. Dai, *J. Mater. Chem. A*, 2013, **1**, 4885–4892.

8 (a) A. Venkateswararao, K. R. J. Thomas, C.-P. Lee, C.-T. Li and K.-C. Ho, *Acs Appl. Mater. Interfaces*, 2014, **6**, 2524–2535; (b) S. Jiang, S. Fan, X. Lu, G. Zhou and Z.-S. Wang, *J. Mater. Chem. A*, 2014, **2**, 1–11.

9 (a) N. Manfredi, B. Cecconi and A. Abbotto, *Eur. J. Org. Chem.*, 2014, **32**, 7069–7086; (b) X. Lu, X. Jia, Z.-S. Wang and G. Zhou, *J. Mater. Chem. A*, 2013, **1**, 9697–9706.

10 (a) A. Abbotto, V. Leandri, N. Manfredi, F. De Angelis, M. Pastore, J. H. Yum, M. K. Nazeeruddin and M. Grätzel, *Eur. J. Org. Chem.*, 2011, **31**, 6195–6205; (b) V. Leandri, R. Ruffo, V. Trifiletti and A. Abbotto, *Eur. J. Org. Chem.*, 2013, **30**, 6793–6801; (c) R. Y.-Y. Lin, F.-L. Wu, C.-H. Chang, H.-H. Chou, T.-M. Chuang, T.-C. Chu, C.-Y. Hsu, P.-W. Chen, K.-C. Ho, Y.-H. Lo and J. T. Lin, *J. Mater. Chem. A*, 2014, **2**, 3092–3101.

11 X. Qian, Y.-Z. Zhu, J. Song, X.-P. Gao and J.-Y. Zheng, *Org. Lett.*, 2013, **15**, 6034–6037.

12 A. Arcadi, M. Chiarini, G. D'Anniballe, F. Marinelli and E. Pietropaolo, *Org. Lett.*, 2014, **16**, 1736–1739.

13 . Y.-Y. Lin, H.-W. Lin, Y.-S. Yen, C.-H. Chang, H.-H. Chou, P.-W. Chen, C.-Y. Hsu, Y.-C. Chen, J. T. Lin and K.-C. Ho, *Energy Environ. Sci.*, 2013, **6**, 2477–2486.

14 Y. Liang, B. Peng, J. Liang, Z. Tao and J. Chen, *Org. Lett.*, 2010, **12**, 1204–1207.

15 P. Gao, H. N. Tsao, M. Grätzel and M. K. Nazeeruddin, *Org. Lett.*, 2012, **14**, 4330–4333.

16 (a) D. Kumar, K. R. J. Thomas, C.-P. Lee and K.-C. Ho, *J. Org. Chem.*, 2014, **79**, 3159–3172; (b) W.-Q. Liu, Z.-G. Liang, D.-X. Kou, L.-H. Hu and S.-Y. Dai, *Electrochim. Acta*, 2013, **88**, 395-403.

17 (a) L.-Y. Chang, C.-P. Lee, R. Vittal, J.-J. Lin and K.-C. Ho, *J. Mater. Chem. A*, 2013, **1**, 3055–3060; (b) H. Choi, S. Paek, K. Lim, C. Kim, M.-S. Kang, K. Song and J. Ko, *J. Mater. Chem. A*, 2013, **1**, 8226–8233. (c) J. Tian, X. Yang, J. Zhao, L. Wang, W. Wang, J. Li and L.. Sun, *RSC Adv.*, 2014, **4**, 34644–34648. (d) X. Yang, J. Zhao, L. Wang, J. Tian and L. Sun, *RSC Adv.*, 2014, **4**, 24377–24383.

18 (a) J. Liu, X. Yang, A. Islam, Y. Numata, S. Zhang, N. T. Salim, H. Chen and L. Han, *J. Mater. Chem. A*, 2013, **1**, 10889–10897; (b) S. Zhu, Z. An, X. Chen, P. Chen and Q. Liu, *RSC Adv.*, 2014, **4**, 42252–42259.

19 (a) L.-Y. Lin, M.-H. Yeh, C.-P. Lee, J. Chang, A. Baheti, R. Vittal, K. R. J. Thomas and K.-C. Ho, *J. Power Sources*, 2014, **247**, 906–914. (b) Z. Wan, C. Jia, Y. Duan, X. Chen, Z. Li and Y. Lin, *RSC Adv.*, 2014, **4**, 34896–34903.

20 G. E. Zervaki, M. S. Roy, M. K. Panda, P. A. Angaridis, E. Chrissos, G. D. Sharma and A. G. Coutsolelos, *Inorg. Chem.*, 2013, **52**, 9813–9825.

Table of contents

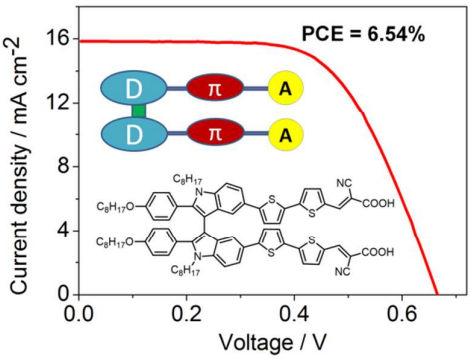

Novel biindole-based double D-π-A branched organic dyes have been designed and synthesized for dye-sensitized solar cells.